

SOLAR: SVD-Optimized Lifelong Attention for Recommendation

Chenghao Zhang^{*1} Chao Feng^{*1} Yuanhao Pu^{*†1} Xunyang Yang^{†1} Wenhui Yu² Xiang Li¹ Yongqi Liu¹
Lantao Hu¹ Kaiqiao Zhan¹ Han Li¹ Kun Gai²

Abstract

Attention mechanism remains the defining operator in Transformers since it provides expressive global credit assignment, yet its $\mathcal{O}(N^2d)$ time and memory cost in sequence length N makes long-context modeling expensive and often forces truncation or other heuristics. Linear attention reduces complexity to $\mathcal{O}(Nd^2)$ by reordering computation through kernel feature maps, but this reformulation drops the softmax mechanism and shifts the attention score distribution. In recommender systems, low-rank structure in matrices is not a rare case, but rather the default inductive bias in its representation learning, particularly explicit in the user behavior sequence modeling. Leveraging this structure, we introduce **SVD-Attention**, which is theoretically lossless on low-rank matrices and preserves softmax while reducing attention complexity from $\mathcal{O}(N^2d)$ to $\mathcal{O}(Ndr)$. With SVD-Attention, we propose **SOLAR**, SVD-Optimized Lifelong Attention for Recommendation, a sequence modeling framework that supports behavior sequences of ten-thousand scale and candidate sets of several thousand items in cascading process without any filtering. In Kuaishou’s online recommendation scenario, SOLAR delivers a 0.68% Video Views gain together with additional business metrics improvements.

1. Introduction

Attention has become the dominant primitive for learning global interactions in modern architectures. The Transformer (Vaswani et al., 2017) replaces recurrence by using attention mechanisms, which enable learning dependencies between elements based on their content, and the same operator now underpins competitive models across modal-

^{*}Equal contribution [†]Work done during an internship at Kuaishou Technology ¹Kuaishou Technology, Beijing, China ²Unaffiliated. Correspondence to: Chao Feng <fengchao08@kuaishou.com>.

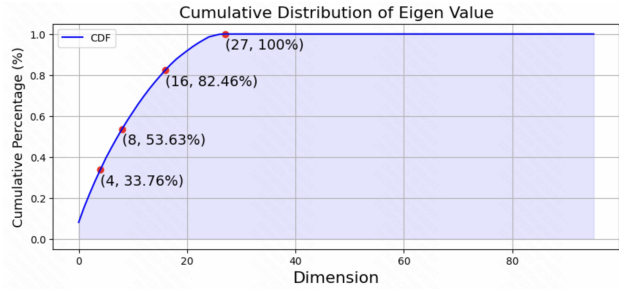


Figure 1. Low rank nature of user sequence representation. This figure shows the cumulative distribution of eigenvalues from SVD decomposition. At rank 27, all information is captured.

ities, including vision systems built on tokenized patches and hierarchical windows (Dosovitskiy et al., 2021; Liu et al., 2021). This success has a concrete cost: standard softmax attention couples expressivity to an $\mathcal{O}(N^2d)$ time and memory footprint in sequence length N , which turns long-context modeling into an engineering problem rather than a modeling choice.

A large body of work (Wang et al., 2020; Kitaev et al., 2020) attempts to decouple accuracy from quadratic scaling, but most solutions quietly change the operator being optimized. Sparse and truncated schemes reduce compute by discarding interactions (Draye et al., 2025), which is often acceptable in tasks where local evidence dominates but becomes fragile when weak signals distributed across the sequence matter. Linear attention (Katharopoulos et al., 2020) takes a more radical route by reordering computations through kernel feature maps, reducing complexity to $\mathcal{O}(Nd^2)$, yet it does so by removing the softmax normalization that shapes attention as a competitive allocation mechanism. The resulting score distribution shift is not cosmetic; it can induce overly smooth attention patterns and systematically underweight high-magnitude keys, an effect analyzed as magnitude neglect (Fan et al., 2025).

Low-rank structure offers a different lever because it targets redundancy in the data geometry rather than approximating the attention rule. This low-rank structure appears in many scenarios: Figure 1 illustrates the low-rank phenomenon in user behavior sequences within recommendation systems. Low-rank factorization is a long-standing tool

for capturing shared latent factors in recommendation and beyond (Koren et al., 2009), and it continues to reappear as a practical bias in large-scale representation learning, including parameter-efficient adaptation (Hu et al., 2022) and attention-side compression strategies in large models (DeepSeek-AI, 2024). For recommender systems, the case for low-rank is not merely aesthetic: scaling analyses show that embedding representations tend to collapse onto low-dimensional subspaces as models grow, producing embedding matrices that behave increasingly like low-rank objects (Guo et al., 2024). This empirical bias suggests that the dominant cost in attention-based sequence modeling is often paid to process redundancy.

The tension is most visible in industrial recommendation pipelines, where models must score large candidate sets against long user histories under strict latency constraints. Target attention architectures such as DIN (Zhou et al., 2018) and DIEN (Zhou et al., 2019) highlight the value of candidate-conditioned sequence aggregation, yet they typically operate on aggressively truncated behavior windows. Systems that push sequence length to the lifelong scale usually rely on retrieval or filtering to keep inference feasible, as illustrated by search-based interest modeling (Pi et al., 2020) and two-stage interest networks (Chang et al., 2023). These mechanisms improve throughput, but they also hard-code a selection policy that can suppress long-tail evidence and entangle modeling quality with the behavior retrieval heuristic.

This paper argues that the efficiency bottleneck can be reduced without abandoning softmax or filtering the sequence by exploiting low-rank structure explicitly. We introduce SVD-attention, which is theoretically lossless on low-rank matrices and preserves softmax while reducing attention complexity from $\mathcal{O}(N^2d)$ to $\mathcal{O}(Ndr)$. Building on this operator, we propose **SOLAR**, **SVD-Optimized Lifelong Attention for Recommendation**, a sequence modeling framework that supports behavior sequences of ten-thousand scale and candidate sets of several thousand items in cascading process, without any filtering. SOLAR is designed for set-conditioned ranking, where the model must assign scores that are meaningful under competition among candidates rather than under independent point-wise evaluation. This perspective aligns with our recently proposed **IFA** (Yu et al., 2024) which proposes set-wise architectures for lifelong behavior modeling, but replaces the distribution-shifting linearization with a low-rank formulation that targets the dominant computational term while maintaining the softmax mechanism. In Section 4.2, we theoretical prove that point-wise models face ranking errors due to structural limits when user preferences are context-dependent and they cannot mitigate the generalization penalty induced by correlation from the perspectives of Ranking Bias and Generalization Gap. In **Kuaishou**'s online deployment scenario,

SOLAR delivers a 0.68% Video Views gain together with additional improvements on other business metrics.

Contributions. Our contributions are as follows:

- We introduce SVD-Attention, a attention mechanism that exploits low-rank structure in the shared key-value matrix, reducing the complexity from $\mathcal{O}(N^2d)$ to $\mathcal{O}(Ndr)$ with rank- r of representations.
- We build SOLAR leveraging SVD-Attention, a set-aware sequence modeling framework for recommendation systems and provide a theoretical analysis that exposes the ranking bias and generalization penalty of point-wise scoring in set-wise recommendation.

Extensive offline benchmarks and online deployment substantiate the approach. Our implemented framework has been deployed in Kuaishou APP, enabling the modeling of historical sequences with lengths on the order of tens of thousands, and contributing to business gains.

2. Related Work

2.1. Attention and Efficient Attention

Transformers (Vaswani et al., 2017) rely on softmax attention to express global interactions, but the quadratic dependence on sequence length has driven a steady stream of efficiency-oriented redesigns. One line of work enforces sparsity or locality in the attention pattern, using restricted receptive fields or sampling to avoid the full $N \times N$ interaction map, as in Longformer (Beltagy et al., 2020) and Reformer (Kitaev et al., 2020). Another line reduces tokens through clustering or low-dimensional projections, with representative examples including Set Transformer (Lee et al., 2019) and Linformer (Wang et al., 2020). Kernelized linear attention (Katharopoulos et al., 2020) removes the softmax normalization to enable associative reordering. These approaches deliver substantial speedups, yet they typically trade exactness for scalability, either by dropping interactions or by changing the normalization that governs how evidence competes. The distributional consequences are now well documented; Fan et al. highlights a concrete failure mode where the reformulation alters attention sharpness and relative weighting in linear attention.

Low-rank structure has also been explored as an efficiency lever, particularly in recommendation systems where user histories exhibit redundancy. LREA (Song et al., 2025) compresses long-term behavior modeling through low-rank decomposition and matrix absorption to reduce serving cost. Our focus differs in the target object: rather than approximating attention through heuristic sparsification or replacing softmax, we derive an SVD-based attention formulation

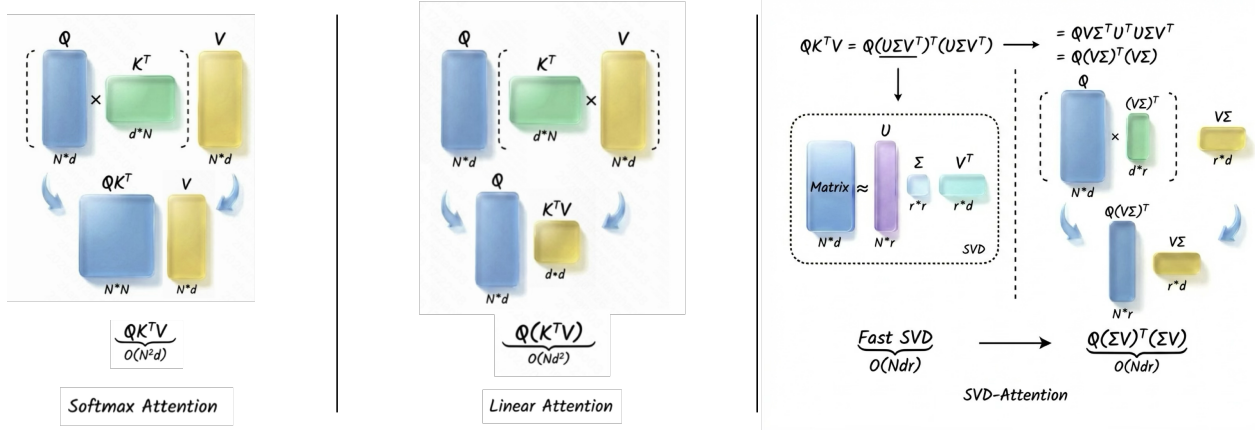


Figure 2. **Overview of Attention Complexity.** Softmax attention explicitly forms the dense attention matrix $QK^T \in \mathbb{R}^{N \times N}$ and then multiplies by V , resulting in $O(N^2d)$ time complexity. Linear attention leverages associativity to rewrite the computation as $Q(K^TV)$, avoiding the $N \times N$ matrix and reducing complexity to $O(Nd^2)$. **SVD-Attention** applies a rank- r SVD ($r \ll d$) to obtain a low-rank factorization. After reassembling the decomposed $U\Sigma V$, the computation of U can theoretically be eliminated, as $U^T U = I$, in low rank representations, which maintains the order of computation as in traditional attention, yielding an overall complexity of $O(Ndr)$.

that is lossless on low-rank matrices and keeps the softmax mechanism intact.

2.2. Sequential Modeling in Recommendation Systems

Attention entered industrial CTR prediction primarily through target attention, where the candidate item queries a user behavior sequence. DIN (Zhou et al., 2018) and DIEN (Zhou et al., 2019) exemplify this design, while self-attentive recommenders such as SASRec (Kang and McAuley, 2018) bring Transformer-style sequence modeling into recommendation and Information Retrieval. The central obstacle in industrial deployments is not modeling flexibility but the product of candidate size and sequence length under millisecond latency budgets, pushing most systems to cap the effective history or to introduce filtering.

Search-based and two-stage pipelines are the prevailing workaround. SIM (Pi et al., 2020) scales to long histories by retrieving relevant behaviors through indexing, and TWIN (Chang et al., 2023) extends this idea with a consistency-preserved two-stage interest model that expands the effective sequence length from 100 to 10^4 – 10^5 . TWIN V2 (Si et al., 2024) further compresses life-cycle histories through hierarchical clustering to accommodate up to 10^6 behaviors. End-to-end alternatives attempt to reduce the mismatch introduced by retrieval heuristics; ETA-Net (Chen et al., 2022) replaces explicit retrieval with hashing-based mechanisms that allow efficient target attention over longer sequences. These systems demonstrate that long behavior is valuable, but the reliance on retrieval, compression, or approximate attention makes the final scorer contingent on a separate selection or aggregation policy.

Candidate-set modeling addresses a different limitation that

becomes salient in cascading ranking scenarios: point-wise scoring treats candidates as independent even though the deployment objective is inherently set-conditioned. IFA (Yu et al., 2024) first formalizes this shift by performing cross-attention between the entire candidate set and the full lifelong behavior sequence, computing candidate-specific signals without filtering and treating the candidate set as a first-class input. This set-wise paradigm is a stronger match to ranking objectives, but its practical deployment still depends on an attention operator that scales and does not distort the score distribution. Recent work also points toward scaling sequence models in recommendation, including LONGER (Chai et al., 2025) and large-model directions motivated by scaling laws and generative recommenders (Zhang et al., 2024; Zhai et al., 2024). Our work targets the core bottleneck shared by these trends: efficient set-wise interaction requires an attention mechanism that can process ten-thousand scale histories and thousand-scale candidate sets without resorting to lossy filtering or distribution-shifting linearization.

3. Preliminaries

Industrial rankers are typically built around per-item scoring. A request includes a user context and a candidate set produced by retrieval or pre-ranking, yet the model scores each candidate in isolation and then sorts by these scores. This point-wise abstraction trades fidelity for convenience: it assumes an item’s relevance can be assessed without reference to the other candidates, which breaks whenever exposure is shared and user choice depends on the co-displayed candidates. Set-wise scoring removes this constraint by allowing an item’s score to depend on the entire candidate set, aligning the scorer with the set-conditioned decision problem the

system actually solves.

Terminology. Consider a set-conditioned ranking problem where each user/context $u \in \mathcal{U}$ is related with a candidate set $X_u = \{x_{u,1}, \dots, x_{u,m}\} \subset \mathcal{X}$. Let $\mathbf{y}_u = [y_{u,1}, \dots, y_{u,m}]^\top \in \{0, 1\}^m$ denote the relevance vector. Assume that (u, X_u, \mathbf{y}_u) is drawn from distribution $\mathcal{D} \sim \mathcal{U} \times \mathcal{X}^m \times \{0, 1\}^m$.

Definition 3.1 (Scoring Functions). A scoring function is a measurable mapping that assigns a real-valued score to each candidate item. We distinguish two types of hypothesis classes: **Point-wise** and **Set-wise** scoring functions.

$$f_{\text{point}} : \mathcal{U} \times \mathcal{X} \rightarrow \mathbb{R}, \quad s_i = f_{\text{point}}(u, x_{u,i}), \quad (1)$$

$$f_{\text{set}} : \mathcal{U} \times \mathcal{X} \times \mathcal{X}^m \rightarrow \mathbb{R}, \quad s_i = f_{\text{set}}(u, x_{u,i}, X_u), \quad (2)$$

The **point-wise** class is general in industrial applications (e.g., Dual-Encoders) due to its inference efficiency, but its local independence structurally prevents modeling contextual features. In contrast, the **set-wise** class allows scores to depend on X at the cost of higher computational complexity.

Given predicted scores s_i , we quantify model performance with Bipartite Ranking Risk, which penalizes misordered positive-negative pairs.

Definition 3.2 (Bipartite Ranking Risk). Let $\mathcal{P} = \{i \mid y_i = 1\}$ and $\mathcal{N} = \{j \mid y_j = 0\}$ be the indices of relevant and irrelevant items, respectively. The ranking error of a scoring function h is:

$$\mathcal{R}(f) = \mathbb{E}_{\mathcal{D}} \left[\frac{1}{|\mathcal{P}||\mathcal{N}|} \sum_{i \in \mathcal{P}} \sum_{j \in \mathcal{N}} \mathbb{I}(s_j \geq s_i) \right], \quad (3)$$

where the term is defined as 0 if $\mathcal{P} = \emptyset$ or $\mathcal{N} = \emptyset$.

Standard results in bipartite ranking theory establish that the optimal ranking is induced by the marginal posterior probability (Menon and Williamson, 2016).

Definition 3.3 (Bayes-optimal Scorer). The Bayes-optimal relevance score $\eta^* : \mathcal{U} \times \mathcal{X} \times \mathcal{X}^m \rightarrow [0, 1]$ is defined as:

$$\eta^*(u, x_{u,i}, X_u) = \mathbb{P}(y_i = 1 \mid u, x_{u,i}, X_u). \quad (4)$$

The scoring function $f^*(u, x_{u,i}, X_u) = \eta^*(u, x_{u,i}, X_u)$ minimizes the pairwise ranking error $\mathcal{R}(f)$.

Attention Mechanism. Let $L, m, d \in \mathbb{N}$ denote the length of the user behavior sequence, the number of candidate items and the embedding dimension. The user history sequence and candidate set are represented as

$$\begin{aligned} H &= [h_1^\top; \dots; h_{N_L}^\top] \in \mathbb{R}^{N_L \times d}, \\ C &= [c_1^\top; \dots; c_{N_C}^\top] \in \mathbb{R}^{N_C \times d}, \end{aligned} \quad (5)$$

where $h_t, c_i \in \mathbb{R}^d$ denote the embeddings of historical and candidate items. The projections are defined as:

$$\text{Query} = CW_Q, \text{Key} = HW_K, \text{Value} = HW_V, \quad (6)$$

where $W_Q, W_K, W_V \in \mathbb{R}^{d \times d}$ are learnable parameters. The standard softmax-attention explicitly constructs the interaction matrix between candidates and historical behaviors. Given Query $\in \mathbb{R}^{N_C \times d}$ and Key $\in \mathbb{R}^{N_L \times d}$, the multiplication Query Key[⊤] incurs a cost of $\mathcal{O}(N^2d)$. The subsequent multiplication with Value $\in \mathbb{R}^{N_L \times d}$ introduces an additional $\mathcal{O}(N^2d)$ term. As a result, the overall computational complexity of softmax-attention scales as $\mathcal{O}(N^2d)$:

$$\text{Attn}_{\text{sm}} : \text{MatMul}(\text{MatMul}(\text{Query}, \text{Key}^\top), \text{Value}). \quad (7)$$

In large-scale recommendation systems, this quadratic dependence on the sequence and candidate sizes becomes a primary bottleneck. Practical models frequently employ linear attention variants that reorder the computation to avoid explicitly forming the $N_C \times N_L$ attention matrix, reducing the complexity to $\mathcal{O}(Nd^2)$, which defines as:

$$\text{Attn}_{\text{lin}} : \text{MatMul}(\text{Query}, \text{MatMul}(\text{Key}^\top, \text{Value})). \quad (8)$$

This reordering discards the softmax normalization, losing its row-stochastic weighting and often harming stability and calibration in ranking, whereas our SVD-attention preserves the original softmax attention order while reducing the computation.

4. Methodology

4.1. SVD-Attention

In attention mechanism, key and value are instantiated from the same matrix. This structure makes the remaining cost largely redundant when the behavior embeddings concentrate in a low-dimensional subspace. This cost is largely avoidable when the behavior embeddings lie close to a low-rank subspace in SVD-Attention.

Let H denote the shared key-value matrix. We compute a rank- r truncated singular value decomposition of H :

$$H = U\Sigma V^\top, U \in \mathbb{R}^{N_L \times r}, \Sigma \in \mathbb{R}^{r \times r}, V \in \mathbb{R}^{d \times r}, \quad (9)$$

with $r \ll \min(N_L, d)$, and $U^\top U = I_r$. Substituting into the attention operator yields

$$\begin{aligned} \text{Key}^\top \text{Value} &= (HW_K)^\top (HW_V) \\ &= (U\Sigma V^\top W_K)^\top (U\Sigma V^\top W_V) \\ &= W_K^\top V\Sigma^\top (U^\top U)\Sigma V^\top W_V \\ &= ((V\Sigma)^\top W_K)^\top (V\Sigma)^\top W_V \end{aligned} \quad (10)$$

where we eliminate the $U \in \mathbb{R}^{N_L \times r}$ and we have:

$$\begin{aligned} \text{Query} &= CW_Q \in \mathbb{R}^{N \times d}, \\ \text{Key}_r &= (V\Sigma)^\top W_K \in \mathbb{R}^{r \times d}, \\ \text{Value}_r &= (V\Sigma)^\top W_V \in \mathbb{R}^{r \times d}. \end{aligned} \quad (11)$$

Substituting this factorization into the attention computation gives same order of traditional attention:

$$\text{Attn}_{\text{SVD}} : \text{MatMul}(\text{MatMul}(\text{Query}, \text{Key}_r^\top), \text{Value}_r) \quad (12)$$

This evaluation avoids forming the dense $d \times d$ product. Computing Query Key_r costs $\mathcal{O}(Ndr)$ and multiplying by Value_r[⊤] costs another $\mathcal{O}(Ndr)$, so the forward complexity is $\mathcal{O}(Ndr)$. A comparison of complexity is given in Table 1.

Table 1. Complexity comparison between attention mechanisms.

Method	Time Complexity
Softmax Attention	$\mathcal{O}(N^2d)$
Linear Attention	$\mathcal{O}(Nd^2)$
SVD Attention (Ours)	$\mathcal{O}(Ndr)$

When $r \ll d$, the SVD-based formulation significantly accelerates the attention computation.

4.1.1. EFFICIENT SVD FORWARD PASS

To avoid the expensive full SVD on $H \in \mathbb{R}^{L \times d}$, we adopt **Randomized-SVD** (Halko et al., 2011) with power iterations and the complexity of $\mathcal{O}(Ndr)$.

Algorithm 1 Randomized SVD with Power Iteration

Require: Matrix $H \in \mathbb{R}^{N_L \times d}$; target rank r ; number of iterations n_{iter} .

Ensure: Singular values $s \in \mathbb{R}^r$ and right singular vectors $R \in \mathbb{R}^{d \times r}$.

Init $\Omega \in \mathbb{R}^{d \times r}$ with $\Omega_{ij} \sim \mathcal{N}(0, 1)$.

for $i = 1$ to n_{iter} **do**

$\Omega \leftarrow H^\top (H\Omega)$ *(power iteration)*

end for

Compute basis Q of $H\Omega$ via QR decomposition.

Compute SVD: $Q^\top H = U_S S R^\top$.

$s \leftarrow \text{diag}(S)$.

Return: s, R .

4.1.2. BACKWARD PASS THROUGH SVD

SVD operation is not trivially differentiable, hence not directly scalable for back propagation. Inspired by the matrix backpropagation framework (Ionescu et al., 2015), consider $H = U\Sigma V^\top$, where $U \in \mathbb{R}^{N_L \times r}$, $\Sigma \in \mathbb{R}^{r \times r}$, $V \in \mathbb{R}^{d \times r}$.

Let the upstream gradients be $\bar{U} = \frac{\partial \mathcal{L}}{\partial U}$, $\bar{\Sigma} = \frac{\partial \mathcal{L}}{\partial \Sigma}$, $\bar{V} = \frac{\partial \mathcal{L}}{\partial V}$. The gradient w.r.t. the input matrix H (within truncated subspace) can be expressed as

$$\begin{aligned} \frac{\partial L}{\partial H} &= \bar{U}\Sigma^{-1}V^\top + U \text{diag} \left(\bar{\Sigma} - U^\top \bar{U}\Sigma^{-1} \right) V^\top \\ &\quad + 2U\Sigma \text{sym} \left(F \circ (V^\top (\bar{V} - V(\bar{U}\Sigma^{-1})^\top U\Sigma)) \right) V^\top \end{aligned} \quad (13)$$

where \circ denotes element-wise product, diag and sym denotes diagonal and symmetric operation. $F \in \mathbb{R}^{r \times r}$ is defined as

$$F_{ij} = \begin{cases} \frac{1}{\sigma_i^2 - \sigma_j^2}, & i \neq j, \\ 0, & i = j, \end{cases} \quad (14)$$

with singular values $\{\sigma_i\}$ on the diagonal of Σ . Since SVD-attention avoids computation of matrix U , we safely conclude that $\bar{U} \equiv 0$ for any orthogonal matrix U , thus

$$\frac{\partial L}{\partial H} = U \left[(\bar{\Sigma})_{\text{diag}} + 2\Sigma \left(F \circ (V^\top \bar{V}) \right)_{\text{sym}} \right] V^\top \quad (15)$$

The detailed process is provided in Appendix B. This formulation provides a stable and well-defined gradient for the SVD operation during training, enabling end-to-end learning with the SVD-accelerated attention mechanism.

4.2. Set-Wise Architectures

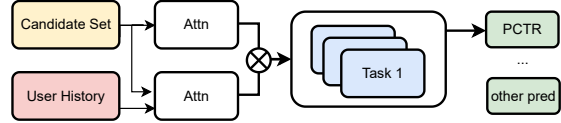


Figure 3. Illustration of SOLAR, an architecture that applies SVD-Attention to historical sequence modeling and includes set-wise modeling of candidate set.

We propose SOLAR, SVD-Optimized Lifelong Attention for Recommendation, an architecture that applies SVD-Attention to historical sequence modeling and includes set-wise modeling of candidate sets, achieving high efficiency in large-scale recommendation tasks. This subsection establishes the theoretical superiority of Set-wise architectures over Point-wise baselines. We analyze from the perspectives of **Ranking Bias** and **Generalization Gap** to prove that:

1. When user preferences are context-dependent, Point-wise models suffer from irreducible ranking errors due to structural limitations;
2. Even trained with List-wise losses, Point-wise models cannot mitigate the generalization penalty induced by correlations.

4.2.1. RANKING BIAS: POINT-WISE BOTTLENECK

The following analysis demonstrate that a point-wise scoring function is incapable of modeling context-dependent relevance even when optimizing a ranking-consistent objective (e.g., pairwise loss). First, we formalize the phenomenon where ground-truth preference reverses due to context changes.

Definition 4.1 (Contextual Flip). $\exists x_i, x_j \in \mathcal{X}$ with two candidate sets $X^{(1)}, X^{(2)} \subset \mathcal{X}$ appearing with non-zero probability, such that:

$$\begin{aligned} \eta^*(x_i, X^{(1)}) &> \eta^*(x_j, X^{(1)}), \\ \eta^*(x_i, X^{(2)}) &< \eta^*(x_j, X^{(2)}). \end{aligned} \quad (16)$$

Definition 4.1 captures a ubiquitous property in realistic scenarios: the relative desirability of item i versus j is not intrinsic but contingent on its surrounding candidates X .

We then evaluate ranking capability via $\mathcal{R}(f)$ in Def. 3.2. Since directly optimizing it is intractable, we consider the standard pairwise surrogate. Let $\pi_{ij}^*(X) = \mathbb{I}(\eta^*(x_i, X) > \eta^*(x_j, X))$ be the ideal preference. For a point-wise scorer $f \in \mathcal{F}_{\text{point}}$, the surrogate population risk is:

$$R(f) = \mathbb{E}_X \left[\sum_{i \neq j} \mathcal{L}_{\text{BCE}}(f(x_i) - f(x_j), \pi_{ij}^*(X)) \right] \quad (17)$$

where \mathcal{L}_{BCE} is the binary cross-entropy loss. The following theorem characterizes the asymptotic limit of a point-wise model trained on this objective (proof in Appendix C.1).

Theorem 4.2 (Bayes Limit of Point-wise Scorers). *Let*

$$p_{ij} = \mathbb{P}(\eta^*(x_i, X) > \eta^*(x_j, X)) = \mathbb{E}_X[\pi_{ij}^*(X)] \quad (18)$$

denote the global marginal preference probability of item i over j . The minimizer $f^* \in \arg \min_{f \in \mathcal{F}_{\text{point}}} R(f)$ satisfies:

$$f^*(x_i) - f^*(x_j) = \log \frac{p_{ij}}{1 - p_{ij}}, \forall i, j, p_{ij} \in (0, 1). \quad (19)$$

Equivalently, $\sigma(f^*(x_i) - f^*(x_j)) = p_{ij}$.

It reveals that a point-wise model collapses context-dependent preferences into a single averaged scalar. This leads to inevitable errors when the local preference in a realized set deviates from the global average.

Corollary 4.3 (Irreducible Ranking Risk(Proof in Appendix C.2)). *Under Assumption 4.1, any point-wise scorer $f_{\text{point}} \in \mathcal{F}_{\text{point}}$ incurs a strictly positive Bipartite Ranking Risk, i.e.,*

$$\mathcal{R}(f_{\text{point}}) > 0. \quad (20)$$

Crucially, this lower bound holds for any pointwise scoring function f_{point} , regardless of its objectives. In contrast, the optimal set-wise scorer $f_{\text{set}}^*(x, X) = \eta^*(x, X)$ achieves zero risk.

4.2.2. GENERALIZATION BOUNDS

Consider a scenario of N requests. For each request $u \in \{1, \dots, N\}$, a candidate set $X_u = \{x_{u,1}, \dots, x_{u,m}\} \subset \mathbb{R}^d$ is provided, with each candidate possessing a binary label $y_{u,i} \in \{0, 1\}$. We focus on a linear scoring head $s_{u,i} = w^\top \phi(u, x_i, X_u$ (if set-wise)) with $\|w\|_2 \leq W$, and assume bounded representations $\|\phi(\cdot)\|_2 \leq B$.

For any tuple $(u, X_u, \mathbf{y}_u) \in \mathcal{D}$ with $s_i = f(u, x_i, X_u)$, let $\ell(\cdot)$ be a 1-Lipschitz loss function w.r.t. s_i and takes values in $[0, 1]$. Denote population and empirical risk by

$$\begin{aligned} R(f) &= \mathbb{E}_{\mathcal{D}} [\ell(f(u, x_i, X_u), y_{u,i})] \\ \hat{R}_S(f) &= \frac{1}{|S|} \sum_{(u,i) \in S} \ell(f(u, x_{u,i}, X_u), y_{u,i}) \end{aligned} \quad (21)$$

where S denotes the training sample set. We utilize the standard bound (Bartlett and Mendelson, 2002): for any hypothesis class \mathcal{F} , with probability at least $1 - \delta$,

$$R(f) \leq \hat{R}_S(f) + 2\mathfrak{R}_S(\ell \circ \mathcal{F}) + 3\sqrt{\frac{\ln(2/\delta)}{2T}}, \quad (22)$$

where T is the number of independent sampling units.

Theorem 4.4 (I.I.D., proof in Appendix C.3). *Assume all training samples (u, i) are i.i.d. drawn. Let $\mathcal{F} = \{(u, x, X) \mapsto w^\top \phi(u, x, X) : \|w\|_2 \leq W, \|\phi(\cdot)\| \leq B\}$. Then the Rademacher complexity satisfies*

$$\mathfrak{R}_S(\ell \circ \mathcal{F}) \leq \frac{WB}{\sqrt{mN}}. \quad (23)$$

Consequently, with probability at least $1 - \delta$, for all $f \in \mathcal{F}$,

$$R(f) - \hat{R}_S(f) \leq \frac{2WB}{\sqrt{mN}} + 3\sqrt{\frac{\ln(2/\delta)}{2mN}}. \quad (24)$$

Theorem 4.5 (Block Dependent, proof in Appendix C.4). *Let $\mathcal{F} = \{(u, x, X) \mapsto w^\top \phi(u, x, X) : \|w\|_2 \leq W, \|\phi(\cdot)\| \leq B\}$. Assume an average correlation condition: for each request u ,*

$$\frac{1}{m(m-1)} \sum_{i \neq j} z_{u,i}^\top z_{u,j} \leq \rho B^2, \quad \rho \in [0, 1], \quad (25)$$

where $z_{u,i} = \phi(u, x_i, X)$. Then the Rademacher complexity satisfies

$$\mathfrak{R}_S(\ell \circ \mathcal{F}) \leq \frac{WB}{\sqrt{mN}} \sqrt{1 + (m-1)\rho}. \quad (26)$$

Consequently, with probability at least $1 - \delta$, for all $f \in \mathcal{F}$,

$$R(f) - \hat{R}_S(f) \leq \frac{2WB}{\sqrt{mN}} \sqrt{1 + (m-1)\rho} + 3\sqrt{\frac{\ln(2/\delta)}{2N}}. \quad (27)$$

Table 2. Main results on RecFlow, MIND, and Kuaishou. An 0.001-level improvement is considered significant for industrial CTR prediction, as supported by experiments in paper (Ma et al., 2018; Si et al., 2024; Wang et al., 2021)

Dataset	Metric	DIN(Recent 50) (Zhou et al., 2018)	SIM (Pi et al., 2020)	LREA (Song et al., 2025)	LONGER (Chai et al., 2025)	TWIN (Chang et al., 2023)	TWINv2 (Si et al., 2024)	IFA (Yu et al., 2024)	SOLAR ours
RecFlow	AUC \uparrow	0.6048	0.6113	0.5695	0.6676	0.6057	0.6178	0.6769	0.6812
	Logloss \downarrow	0.0689	0.0673	0.1475	0.0638	0.0687	0.0691	0.0615	0.0610
MIND	AUC \uparrow	0.5909	0.6193	0.6211	0.6355	0.6480	0.6377	0.6697	0.6713
	Logloss \downarrow	0.1324	0.1156	0.1065	0.1137	0.1075	0.1164	0.1060	0.1052
Kuaishou	AUC($mean \pm std$) \uparrow	0.8417 \pm 0.00487	0.8458 \pm 0.00512	0.8479 \pm 0.00523	0.8511 \pm 0.00413	0.8507 \pm 0.00508	0.8492 \pm 0.00492	0.8518 \pm 0.00569	0.8531 \pm 0.00589
	UAUC($mean \pm std$) \uparrow	0.8398 \pm 0.00475	0.8439 \pm 0.00515	0.8460 \pm 0.00519	0.8486 \pm 0.00405	0.8488 \pm 0.00495	0.8473 \pm 0.00487	0.8489 \pm 0.00504	0.8502 \pm 0.00530

Corollary 4.6 (Mismatch factor and extreme regimes). *Under the same conditions,*

$$\frac{\mathfrak{R}_{\text{dep}}}{\mathfrak{R}_{\text{i.i.d}}} \simeq \sqrt{1 + (m - 1)\rho}. \quad (28)$$

We then analyze whether optimizing a Listwise loss can circumvent the penalty derived in Corollary 4.6. Let $\mathcal{P}_u = \{i : y_{u,i} = 1\}$ be the set of positive items for user u . The loss is defined as the average negative log-likelihood of the positive items:

$$\begin{aligned} \ell_{\text{list}}(s; \mathcal{P}_u) &= -\frac{1}{|\mathcal{P}_u|} \sum_{i \in \mathcal{P}_u} \log \left(\frac{\exp(s_i)}{\sum_{j=1}^m \exp(s_j)} \right) \\ &= -\frac{1}{|\mathcal{P}_u|} \sum_{i \in \mathcal{P}_u} s_i + \log \left(\sum_{j=1}^m \exp(s_j) \right). \end{aligned} \quad (29)$$

Lemma 4.7 (Lipschitz Continuity, proof in Appendix C.5). ℓ_{list} is L -Lipschitz w.r.t. s in ℓ_2 -norm, where $L \leq \sqrt{2}$.

Corollary 4.8 (Listwise Generalization Gap). *Let $\mathcal{C}(m, \rho) = \sqrt{1 + (m - 1)\rho}$, then for any hypothesis class trained with Softmax loss, the generalization gap is bounded by:*

$$R(f) - \hat{R}_S(f) \lesssim \frac{2\sqrt{2}WB}{\sqrt{mN}} \mathcal{C}(m, \rho) + \mathcal{O}\left(\frac{1}{\sqrt{N}}\right). \quad (30)$$

Now that the average pairwise correlation ρ governs the generalization error, which scales with $\mathcal{C}(m, \rho)$. This theoretical insight establishes that minimizing feature correlation is necessary for reducing generalization gap. Consequently, we investigate the capabilities of different scoring architectures in managing this correlation.

Consider a pair of items (i, j) within a candidate list. Let $x_i, x_j \in \mathbb{R}^d$ denote input feature vectors. In ranking scenarios, items retrieved by the same request often share a dominant feature. We decompose them as:

$$x_k = \mathbf{c} + \mathbf{d}_k, \quad k \in \{i, j\} \quad (31)$$

where \mathbf{c} represents the shared feature and \mathbf{d}_k the item-specific discriminative feature. Assume that $\|\mathbf{c}\| \gg \|\mathbf{d}_k\|$. Minimizing ℓ_{list} to distinguish i from j is equivalent to maximizing the score margin $\Delta s = s_i - s_j$.

Theorem 4.9 (Correlation Coefficients, proof in Appendix C.6). *Given highly correlated inputs x_i, x_j , the output correlation of the pointwise model (ρ_{point}) is lower-bounded by the input smoothness, whereas the setwise model (ρ_{set}) can asymptotically approach zero through orthogonal projection. Specifically:*

$$\rho_{\text{set}} \ll \rho_{\text{point}} \quad (32)$$

To conclude, our theoretical analysis establishes the fundamental superiority of set-wise architectures from two complementary perspectives. While point-wise models suffer from irreducible ranking errors under contextual flips and loose generalization bounds due to correlations, set-wise models provably eliminate these biases and achieve tighter generalization limits by dynamically de-correlating representations. These results provide new understanding perspectives of context-aware modeling in ranking systems.

5. Evaluation

In this Section, we evaluate SOLAR compared with other common user-behavior modeling framework in industrial recommendation systems through extensive offline and large-scale industrial online experiments.

Table 3. Evaluation settings. Offline benchmarks use length-50 histories and 50-item candidate sets per request. Industrial reports online AUC with 12,000 historical behaviors and 3000 candidates.

Dataset	Evaluation	History length	Candidate size
RecFlow	Offline	50	120
MIND	Offline	50	50-130
Kuaishou	Online	12,000	3000

Benchmark. RecFlow (Liu et al., 2025) and MIND (Wu et al., 2020) serve as offline benchmarks. Each instance contains a length-50 history sequence and around 50-130 candidate set, constructed by the procedure described in Appendix D. Experiment on Kuaishou’s platform is evaluated online using AUC from real training, where each request contains 12 thousands historical behaviors and 3000 candidates. We report Logloss and AUC on RecFlow and MIND. Online experiment reports AUC and UAUC for 24 hours after the model converges during streaming training.

Baseline Setting. Two-stage baselines such as SIM (Pi et al., 2020) apply an explicit filtering stage before scoring. On RecFlow and MIND, they select a subset from the length-50 history and model the top 20 retrieved behaviors. On Kuaishou’s online experiment, they select from the 12,000 length history and model 300 behaviors per request. Other baseline frameworks stay follow the same setting with SOLAR.

5.1. Main results

Table 2 reports the main comparison on RecFlow, MIND, and Kuaishou’s online traffic. On the two offline benchmarks, SOLAR attains the best AUC and Logloss across all methods. On RecFlow, SOLAR reaches an AUC of 0.6812 and a Logloss of 0.0610. On MIND, SOLAR achieves 0.6713 AUC and 0.1052 Logloss. On Kuaishou, SOLAR delivers the best online ranking quality. It achieves AUC 0.8531 and UAUC 0.8502 on real requests. While another set-aware framework IFA (Yu et al., 2024) and SOLAR exhibit very close AUC on all three datasets, Section 5.3 shows that SOLAR attains this accuracy with a more efficient attention operator and reduced machine consumption in the online deployment.

5.2. Forward-pass efficiency of attention

We report the forward cost of the attention kernel and compare Softmax Attention, Linear Attention, and SVD-Attention. To avoid conflating algorithmic scaling with parallel scheduling effects, we run the benchmark on CPU and constrain execution to a single thread. Figure 4 reports forward latency. The plot is intended to expose scaling behavior in the same input regime used by our benchmarks.

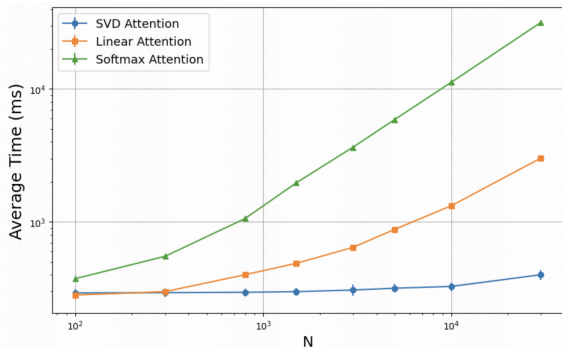


Figure 4. Forward latency of the attention module on CPU under single-thread execution. The x-axis varies the history length N and the y-axis is the time in milliseconds. Candidate size m and embedding dimension d are held fixed.

5.3. Ablation studies

In this ablation study, we keep the overall framework fixed and only swap the attention operator. This design aims to

verify whether any observed changes are attributable to the attention mechanism rather than architectural drift. Additionally, since industrial feasibility is influenced by resource footprint, we also report the number of machines served in the online deployment. The machines deployed online uses CPU. We report number of cores tested under 6.14% real traffic as machine consumption. The machine consumption for online serving not only includes the forward propagation time but also the actual overhead of fetching embeddings and other related operations. Moreover, the SOLAR model is designed around two modeling components: candidate-set modeling and history-sequence modeling. We conducted ablation experiments on these two components to directly assess whether the added structure is truly necessary in the target environments. The AUC results are reported for the RecFlow and Industrial datasets.

Table 4. Attention ablation under a same set-aware framework.

Dataset	RecFlow	Kuaishou	
		AUC	AUC (mean±std) Δ Cores Usage
Softmax Attn(Vaswani et al., 2017)	0.6829	0.8533±0.00451	base
MALA(Fan et al., 2025)	0.6759	0.8525±0.00410	-38.09%
Longformer(Beltagy et al., 2020)	0.6708	0.8539±0.00493	-23.80%
Hiformer (Gui et al., 2023)	0.6718	0.8312±0.00293	-23.80%
Linear Attn(Katharopoulos et al., 2020)	0.6769	0.8518±0.00569	-38.09%
SVD-Attn without Softmax	0.6757	0.8520±0.00656	-
Only Candidate-Set Modeling	0.6293	0.8012±0.00408	-
Only User-History Modeling	0.6644	0.8508±0.00496	-
SVD-Attention	0.6812	0.8531±0.00589	-52.38%

6. Conclusion

Attention mechanism is key in Transformers for global credit assignment, but its $\mathcal{O}(N^2d)$ cost makes long-context modeling expensive. Substitute methods like Linear attention achieves sub-quadratic complexity by reordering the multiplication in traditional attention through kernel feature maps, but the reordering removes softmax and alters the attention score distribution. This paper takes a different route. We derive SVD-attention from the low-rank structure of the shared key-value matrix, and the derivation preserves the conventional QKV multiplication order rather than replacing the operator. SVD-attention is theoretically reduces the dominant attention cost from $\mathcal{O}(N^2d)$ to $\mathcal{O}(Ndr)$ with rank- r while retaining softmax. SVD-attention makes set-conditioned ranking with lifelong histories operational in an industrial recommender. Building on it, SOLAR models user behavior sequences at the ten-thousand scale and scores several thousand candidates in a cascading process without filtering. Theoretical analysis further distinguishes SOLAR from point-wise scoring. While this work evaluates it only for sequential recommendation and does not analyze its behavior in language modeling, vision, or long-context retrieval, we are confident that the underlying design will transfer because low-rank structure is a recurring inductive bias in large-scale representation learning and attention re-

mains the dominant mechanism for global credit assignment, so the same SVD-based acceleration can remove quadratic bottlenecks and provide the community with a practical route to scale modeling beyond recommendation systems.

Impact Statement

This paper aims to advance machine learning by improving the computational scalability of attention through SVD-ATTENTION and by enabling efficient set-wise sequential modeling in recommendation. The contribution is primarily technical, reducing computation and latency under a low-rank regime while preserving the standard attention operator. Any broader societal effects are mediated by downstream applications and deployment choices, none of which we feel must be specifically highlighted here.

References

- Peter L. Bartlett and Shahar Mendelson. 2002. Rademacher and Gaussian Complexities: Risk Bounds and Structural Results. *J. Mach. Learn. Res.* 3 (2002), 463–482. <https://jmlr.org/papers/v3/bartlett02a.html>
- Iz Beltagy, Matthew E. Peters, and Arman Cohan. 2020. Longformer: The Long-Document Transformer. arXiv:2004.05150 <https://arxiv.org/abs/2004.05150>
- Zheng Chai, Qin Ren, Xijun Xiao, Huizhi Yang, Bo Han, Sijun Zhang, Di Chen, Hui Lu, Wenlin Zhao, Lele Yu, Xionghang Xie, Shiru Ren, Xiang Sun, Yaocheng Tan, Peng Xu, Yuchao Zheng, and Di Wu. 2025. LONGER: Scaling Up Long Sequence Modeling in Industrial Recommenders. 247–256 pages. doi:10.1145/3705328.3748065
- Jianxin Chang, Chenbin Zhang, Zhiyi Fu, Xiaoxue Zang, Lin Guan, Jing Lu, Yiqun Hui, Dewei Leng, Yanan Niu, Yang Song, and Kun Gai. 2023. TWIN: Two-stage Interest Network for Lifelong User Behavior Modeling in CTR Prediction at Kuaishou. 3785–3794 pages. doi:10.1145/3580305.3599922
- Qiwei Chen, Yue Xu, Changhua Pei, Shanshan Lv, Tao Zhuang, and Junfeng Ge. 2022. Efficient Long Sequential User Data Modeling for Click-Through Rate Prediction. arXiv:2209.12212 doi:10.48550/ARXIV.2209.12212
- DeepSeek-AI. 2024. DeepSeek-V2: A Strong, Economical, and Efficient Mixture-of-Experts Language Model. arXiv:2405.04434 doi:10.48550/ARXIV.2405.04434
- Alexey Dosovitskiy, Lucas Beyer, Alexander Kolesnikov, Dirk Weissenborn, Xiaohua Zhai, Thomas Unterthiner, Mostafa Dehghani, Matthias Minderer, Georg Heigold, Sylvain Gelly, Jakob Uszkoreit, and Neil Houlsby. 2021. An Image is Worth 16x16 Words: Transformers for Image Recognition at Scale. <https://openreview.net/forum?id=YicbFdNTTy>
- Florent Draye, Anson Lei, Ingmar Posner, and Bernhard Schölkopf. 2025. Sparse Attention Post-Training for Mechanistic Interpretability. arXiv:2512.05865 doi:10.48550/ARXIV.2512.05865
- Qihang Fan, Huaibo Huang, Yuang Ai, and Ran He. 2025. Rectifying Magnitude Neglect in Linear Attention. arXiv:2507.00698 doi:10.48550/ARXIV.2507.00698
- Huan Gui, Ruoxi Wang, Ke Yin, Long Jin, Maciej Kula, Taibai Xu, Lichan Hong, and Ed H. Chi. 2023. Hiformer: Heterogeneous Feature Interactions Learning with Transformers for Recommender Systems. arXiv:2311.05884 doi:10.48550/ARXIV.2311.05884
- Xingzhuo Guo, Junwei Pan, Ximei Wang, Baixu Chen, Jie Jiang, and Mingsheng Long. 2024. On the Embedding Collapse when Scaling up Recommendation Models. <https://openreview.net/forum?id=aPVwOAr1aW>
- Nathan Halko, Per-Gunnar Martinsson, and Joel A. Tropp. 2011. Finding Structure with Randomness: Probabilistic Algorithms for Constructing Approximate Matrix Decompositions. *SIAM Rev.* 53, 2 (2011), 217–288. doi:10.1137/090771806
- Edward J. Hu, Yelong Shen, Phillip Wallis, Zeyuan Allen-Zhu, Yuanzhi Li, Shean Wang, Lu Wang, and Weizhu Chen. 2022. LoRA: Low-Rank Adaptation of Large Language Models. <https://openreview.net/forum?id=nZeVKeeFYf9>
- Catalin Ionescu, Orestis Vantzos, and Cristian Sminchisescu. 2015. Training Deep Networks with Structured Layers by Matrix Backpropagation. *CoRR* abs/1509.07838 (2015). arXiv:1509.07838 <http://arxiv.org/abs/1509.07838>
- Wang-Cheng Kang and Julian J. McAuley. 2018. Self-Attentive Sequential Recommendation. 197–206 pages. doi:10.1109/ICDM.2018.00035
- Angelos Katharopoulos, Apoorv Vyas, Nikolaos Pappas, and François Fleuret. 2020. Transformers are RNNs: Fast Autoregressive Transformers with Linear Attention. 5156–5165 pages. <http://proceedings.mlr.press/v119/katharopoulos20a.html>

- Nikita Kitaev, Lukasz Kaiser, and Anselm Levskaya. 2020. Reformer: The Efficient Transformer. <https://openreview.net/forum?id=rkgNKkHtvB>
- Yehuda Koren, Robert M. Bell, and Chris Volinsky. 2009. Matrix Factorization Techniques for Recommender Systems. *Computer* 42, 8 (2009), 30–37. doi:10.1109/MC.2009.263
- Juho Lee, Yoonho Lee, Jungtaek Kim, Adam R. Kosiorek, Seungjin Choi, and Yee Whye Teh. 2019. Set Transformer: A Framework for Attention-based Permutation-Invariant Neural Networks. 3744–3753 pages. <http://proceedings.mlr.press/v97/lee19d.html>
- Qi Liu, Kai Zheng, Rui Huang, Wuchao Li, Kuo Cai, Yuan Chai, Yanan Niu, Yiqun Hui, Bing Han, Na Mou, Hongning Wang, Wentian Bao, Yunen Yu, Guorui Zhou, Han Li, Yang Song, Defu Lian, and Kun Gai. 2025. RecFlow: An Industrial Full Flow Recommendation Dataset. In *The Thirteenth International Conference on Learning Representations, ICLR 2025, Singapore, April 24-28, 2025*. OpenReview.net. <https://openreview.net/forum?id=vVhc8bGRns>
- Ze Liu, Yutong Lin, Yue Cao, Han Hu, Yixuan Wei, Zheng Zhang, Stephen Lin, and Baining Guo. 2021. Swin Transformer: Hierarchical Vision Transformer using Shifted Windows. 9992–10002 pages. doi:10.1109/ICCV48922.2021.00986
- Xiao Ma, Liqin Zhao, Guan Huang, Zhi Wang, Zelin Hu, Xiaoqiang Zhu, and Kun Gai. 2018. Entire Space Multi-Task Model: An Effective Approach for Estimating Post-Click Conversion Rate. (2018), 1137–1140. doi:10.1145/3209978.3210104
- Aditya Krishna Menon and Robert C. Williamson. 2016. Bipartite Ranking: a Risk-Theoretic Perspective. *J. Mach. Learn. Res.* 17 (2016), 195:1–195:102. <https://jmlr.org/papers/v17/14-265.html>
- Qi Pi, Guorui Zhou, Yujing Zhang, Zhe Wang, Lejian Ren, Ying Fan, Xiaoqiang Zhu, and Kun Gai. 2020. Search-based User Interest Modeling with Lifelong Sequential Behavior Data for Click-Through Rate Prediction. 2685–2692 pages. doi:10.1145/3340531.3412744
- Zihua Si, Lin Guan, Zhongxiang Sun, Xiaoxue Zang, Jing Lu, Yiqun Hui, Xingchao Cao, Zeyu Yang, Yichen Zheng, Dewei Leng, Kai Zheng, Chenbin Zhang, Yanan Niu, Yang Song, and Kun Gai. 2024. TWIN V2: Scaling Ultra-Long User Behavior Sequence Modeling for Enhanced CTR Prediction at Kuaishou. In *Proceedings of the 33rd ACM International Conference on Information and Knowledge Management, CIKM 2024, Boise, ID, USA, October 21-25, 2024*, Edoardo Serra and Francesca Spezzano (Eds.). ACM, 4890–4897. doi:10.1145/3627673.3680030
- Xin Song, Xiaochen Li, Jinxin Hu, Hong Wen, Zulong Chen, Yu Zhang, Xiaoyi Zeng, and Jing Zhang. 2025. LREA: Low-Rank Efficient Attention on Modeling Long-Term User Behaviors for CTR Prediction. In *Proceedings of the 48th International ACM SIGIR Conference on Research and Development in Information Retrieval, SIGIR 2025, Padua, Italy, July 13-18, 2025 (SIGIR '25)*, Nicola Ferro, Maria Maistro, Gabriella Pasi, Omar Alonso, Andrew Trotman, and Suzan Verberne (Eds.). ACM, 2843–2847. doi:10.1145/3726302.3730228
- Ashish Vaswani, Noam Shazeer, Niki Parmar, Jakob Uszkoreit, Llion Jones, Aidan N. Gomez, Lukasz Kaiser, and Illia Polosukhin. 2017. Attention is All you Need. 5998–6008 pages. <https://proceedings.neurips.cc/paper/2017/hash/3f5ee243547dee91fbd053c1c4a845aa-Abstract.html>
- Ruoxi Wang, Rakesh Shivanna, Derek Zhiyuan Cheng, Sagar Jain, Dong Lin, Lichan Hong, and Ed H. Chi. 2021. DCN V2: Improved Deep & Cross Network and Practical Lessons for Web-scale Learning to Rank Systems. In *WWW '21: The Web Conference 2021, Virtual Event / Ljubljana, Slovenia, April 19-23, 2021*, Jure Leskovec, Marko Grobelnik, Marc Najork, Jie Tang, and Leila Zia (Eds.). ACM / IW3C2, 1785–1797. doi:10.1145/3442381.3450078
- Sinong Wang, Belinda Z. Li, Madian Khabza, Han Fang, and Hao Ma. 2020. Linformer: Self-Attention with Linear Complexity. arXiv:2006.04768 <https://arxiv.org/abs/2006.04768>
- Fangzhao Wu, Ying Qiao, Jiun-Hung Chen, Chuhan Wu, Tao Qi, Jianxun Lian, Danyang Liu, Xing Xie, Jianfeng Gao, Winnie Wu, and Ming Zhou. 2020. MIND: A Large-scale Dataset for News Recommendation. In *Proceedings of the 58th Annual Meeting of the Association for Computational Linguistics, ACL 2020, Online, July 5-10, 2020*, Dan Jurafsky, Joyce Chai, Natalie Schluter, and Joel R. Tetraault (Eds.). Association for Computational Linguistics, 3597–3606. doi:10.18653/V1/2020.ACL-MAIN.331
- Wenhui Yu, Chao Feng, Yanze Zhang, Lantao Hu, Peng Jiang, and Han Li. 2024. IFA: Interaction Fidelity Attention for Entire Lifelong Behaviour Sequence Modeling. *CoRR* abs/2406.09742 (2024). arXiv:2406.09742 doi:10.48550/ARXIV.2406.09742
- Jiaqi Zhai, Lucy Liao, Xing Liu, Yueming Wang, Rui Li, Xuan Cao, Leon Gao, Zhaojie Gong, Fangda Gu, Jiayuan He, Yinghai Lu, and Yu Shi. 2024. Actions

Speak Louder than Words: Trillion-Parameter Sequential Transducers for Generative Recommendations. <https://openreview.net/forum?id=xye7iNsgXn>

Buyun Zhang, Liang Luo, Yuxin Chen, Jade Nie, Xi Liu, Shen Li, Yanli Zhao, Yuchen Hao, Yantao Yao, Ellie Dingqiao Wen, Jongsoo Park, Maxim Naumov, and Wenlin Chen. 2024. Wukong: Towards a Scaling Law for Large-Scale Recommendation. <https://openreview.net/forum?id=8iUgr2nuwo>

Guorui Zhou, Na Mou, Ying Fan, Qi Pi, Weijie Bian, Chang Zhou, Xiaoqiang Zhu, and Kun Gai. 2019. Deep Interest Evolution Network for Click-Through Rate Prediction. 5941–5948 pages. doi:10.1609/AAAI.V33I01.33015941

Guorui Zhou, Xiaoqiang Zhu, Chengru Song, Ying Fan, Han Zhu, Xiao Ma, Yanghui Yan, Junqi Jin, Han Li, and Kun Gai. 2018. Deep Interest Network for Click-Through Rate Prediction. In *Proceedings of the 24th ACM SIGKDD International Conference on Knowledge Discovery & Data Mining, KDD 2018, London, UK, August 19-23, 2018*, Yike Guo and Faisal Farooq (Eds.). ACM, 1059–1068. doi:10.1145/3219819.3219823

A. Reproducibility

The code will be published upon acceptance.

B. Detailed Derivation of SVD Gradients

In this section, we provide a derivation of the SVD gradient with respect to the input matrix H , under the constraints of our truncated SVD-Attention mechanism.

B.1. Differential of the SVD

Let $H_r = U\Sigma V^\top$ be the rank- r approximation of $H \in \mathbb{R}^{L \times d}$, then:

$$dH_r = dU\Sigma V^\top + U d\Sigma V^\top + U\Sigma dV^\top. \quad (33)$$

Since U and V are orthogonal matrices, differentiating the identity $U^\top U = I$ yields $(dU)^\top U + U^\top dU = 0$. Defining $\Omega_U = U^\top dU$ and $\Omega_V = V^\top dV$, it follows that Ω_U and Ω_V are skew-symmetric. Thus express the differentials as:

$$dU = U\Omega_U, \quad dV = V\Omega_V. \quad (34)$$

Substituting Eq. (34) into Eq. (33), we obtain:

$$dH_r = U\Omega_U\Sigma V^\top + U d\Sigma V^\top - U\Sigma\Omega_V V^\top. \quad (35)$$

To isolate components $(d\Sigma, \Omega_U, \Omega_V)$, we define the projected differential matrix dP as:

$$dP := U^\top dH_r V = \Omega_U \Sigma + d\Sigma - \Sigma \Omega_V. \quad (36)$$

B.2. Solving the Linear System

As for the (i, j) -th entry of Eq.(36):

$$dP_{ij} = (\Omega_U)_{ij}\sigma_j + d\Sigma_{ij} - \sigma_i(\Omega_V)_{ij}. \quad (37)$$

Noting that diagonal entries of skew-symmetric matrices are zero, and $d\Sigma$ is diagonal, we have:

$$dP_{ij} = \begin{cases} d\Sigma_{ii}, & i = j \\ (\Omega_U)_{ij}\sigma_j - \sigma_i(\Omega_V)_{ij}, & i \neq j \end{cases}. \quad (38)$$

For the off-diagonal case $(i \neq j)$, we consider the transposed projection dP^\top . With property $\Omega^\top = -\Omega$, we derive:

$$dP_{ji} = (dP^\top)_{ij} = -\sigma_i(\Omega_U)_{ij} + \sigma_j(\Omega_V)_{ij}. \quad (39)$$

Combining Eq. (38) and Eq. (39), we obtain two linear equations. Since our attention mechanism does not explicitly instantiate U in the forward pass, eliminating $(\Omega_U)_{ij}$ yields the solution for Ω_V :

$$(\Omega_V)_{ij} = \frac{\sigma_i dP_{ij} + \sigma_j dP_{ji}}{\sigma_j^2 - \sigma_i^2} = \frac{\sigma_i dP_{ij} + \sigma_j dP_{ji}}{-(\sigma_i^2 - \sigma_j^2)}. \quad (40)$$

B.3. Derivation of the Gradient Matrix

We now relate these differentials to the loss function \mathcal{L} . Let the upstream gradients be $\bar{U} = \partial\mathcal{L}/\partial U$, $\bar{\Sigma} = \partial\mathcal{L}/\partial\Sigma$, and $\bar{V} = \partial\mathcal{L}/\partial V$. The total differential of the loss is:

$$d\mathcal{L} = \text{Tr}(\bar{U}^\top dU) + \text{Tr}(\bar{\Sigma}^\top d\Sigma) + \text{Tr}(\bar{V}^\top dV). \quad (41)$$

We have $\bar{U} \equiv 0$ due to its absence in forward pass. Substituting $dV = V\Omega_V$, the equation simplifies to:

$$d\mathcal{L} = \text{Tr}(\bar{\Sigma}^\top d\Sigma) + \text{Tr}(P^\top \Omega_V), \quad (42)$$

where $P = V^\top \bar{V}$. Expanding the trace sum:

$$d\mathcal{L} = \sum_i \bar{\Sigma}_{ii} d\Sigma_{ii} + \sum_{i \neq j} P_{ji} (\Omega_V)_{ij}. \quad (43)$$

Substituting the solution for $(\Omega_V)_{ij}$ from Eq. (40):

$$d\mathcal{L} = \sum_i \bar{\Sigma}_{ii} dP_{ii} - \sum_{i \neq j} P_{ji} \left(\frac{\sigma_i dP_{ij} + \sigma_j dP_{ji}}{\sigma_i^2 - \sigma_j^2} \right). \quad (44)$$

We rearrange the second term to identify the coefficient of dP_{ij} . By swapping indices i and j in the second part of the summation, we derive:

$$\begin{aligned} \text{Sum}_{i \neq j} &= \sum_{i \neq j} \left(-\frac{P_{ji} \sigma_i}{\sigma_i^2 - \sigma_j^2} dP_{ij} - \frac{P_{ji} \sigma_j}{\sigma_i^2 - \sigma_j^2} dP_{ji} \right) \\ &= \sum_{i \neq j} \left(-\frac{P_{ji} \sigma_i}{\sigma_i^2 - \sigma_j^2} + \frac{P_{ij} \sigma_i}{\sigma_i^2 - \sigma_j^2} \right) dP_{ij} \\ &= \sum_{i \neq j} \frac{\sigma_i (P_{ij} - P_{ji})}{\sigma_i^2 - \sigma_j^2} dP_{ij}. \end{aligned} \quad (45)$$

Thus, we can define the gradient matrix $G = \frac{\partial \mathcal{L}}{\partial P}$ such that $d\mathcal{L} = \text{Tr}(G^\top dP)$. The elements of G are:

$$G_{ij} = \begin{cases} \bar{\Sigma}_{ii}, & i = j \\ \sigma_i F_{ij} (P_{ij} - P_{ji}), & i \neq j \end{cases} \quad (46)$$

where $F_{ij} = 1/(\sigma_i^2 - \sigma_j^2)$.

To align with our implementation which utilizes symmetric matrix operations, we observe that the derived term matches the structure of $2\sigma_i \text{sym}(F \circ P)_{ij}$. Using the skew-symmetry $F_{ji} = -F_{ij}$:

$$2 \text{sym}(F \circ P)_{ij} = (F \circ P)_{ij} + (F \circ P)_{ji} = F_{ij} P_{ij} + F_{ji} P_{ji} = F_{ij} (P_{ij} - P_{ji}). \quad (47)$$

Multiplying by σ_i , we recover the derived gradient form. Since we have identified the gradient w.r.t P : $G = \frac{\partial \mathcal{L}}{\partial P}$, where $dP = U^\top dH_r V$, we then apply the chain rule:

$$d\mathcal{L} = \text{Tr}(G^\top dP) = \text{Tr}(G^\top U^\top dH_r V) = \text{Tr}((UGV^\top)^\top dH_r). \quad (48)$$

Thus, the gradient w.r.t H_r is:

$$\frac{\partial \mathcal{L}}{\partial H_r} = UGV^\top = U [\bar{\Sigma}_{\text{diag}} + 2\Sigma \text{sym}(F \circ (V^\top \bar{V}))] V^\top. \quad (49)$$

B.4. Bias Derivation

We further analyze the bias of the gradients derived from rank- r subspace against full-SVD results(Ionescu et al., 2015). Let the full-SVD of $H \in \mathbb{R}^{L \times d}$ be $H = \mathbf{U} \Sigma \mathbf{V}^\top$, where:

$$\mathbf{U} = [U \mid U_\perp], \Sigma = \begin{bmatrix} \Sigma & 0 \\ 0 & \Sigma_\perp \end{bmatrix}, \mathbf{V} = [V \mid V_\perp]. \quad (50)$$

Here, the complements $U_\perp \in \mathbb{R}^{L \times (L-r)}$, $\Sigma_\perp \in \mathbb{R}^{(L-r) \times (d-r)}$, and $V_\perp \in \mathbb{R}^{d \times (d-r)}$. Considering that $\bar{\mathbf{U}} \equiv 0$, the partial differential of the loss \mathcal{L} w.r.t H is:

$$\frac{\partial \mathcal{L}}{\partial H} = \mathbf{U} \mathbf{G} \mathbf{V}^\top = \mathbf{U} [\bar{\Sigma}_{\text{diag}} + 2\Sigma \text{sym}(\mathbf{F} \circ (\mathbf{V}^\top \bar{\mathbf{V}}))] \mathbf{V}^\top. \quad (51)$$

We decompose the gradient matrix \mathbf{G} into blocks corresponding to top- r and the other interactions:

$$\mathbf{G} = \begin{bmatrix} G_{r,r} & G_{r,\perp} \\ G_{\perp,r} & G_{\perp,\perp} \end{bmatrix}. \quad (52)$$

Expanding the full gradient using these blocks:

$$\nabla_H \mathcal{L} = [U \mid U_\perp] \begin{bmatrix} G_{r,r} & G_{r,\perp} \\ G_{\perp,r} & G_{\perp,\perp} \end{bmatrix} \begin{bmatrix} V^\top \\ V_\perp^\top \end{bmatrix} = U G_{r,r} V^\top + \text{Res}. \quad (53)$$

where

$$\text{Res} = U_\perp G_{\perp,r} V^\top + U G_{r,\perp} V_\perp^\top + U_\perp G_{\perp,\perp} V_\perp^\top. \quad (54)$$

The first term corresponds exactly to $\partial \mathcal{L} / \partial H_r$. Approximation bias arises from other blocks, which is carefully derived in following discussions. Consider the blocks of $\mathbf{V}^\top \bar{\mathbf{V}}$:

$$\mathbf{V}^\top \bar{\mathbf{V}} = \begin{bmatrix} V^\top \\ V_\perp^\top \end{bmatrix} [\bar{V} \mid \bar{V}_\perp] = \begin{bmatrix} V^\top \bar{V} & V^\top \bar{V}_\perp \\ V_\perp^\top \bar{V} & V_\perp^\top \bar{V}_\perp \end{bmatrix} \quad (55)$$

then the three blocks in \mathbf{G} can be expressed as:

$$\begin{aligned} G_{r,\perp} &= \Sigma \cdot \mathbf{F}_{r,\perp} \circ (V^\top \bar{V}_\perp + \bar{V}^\top V_\perp) \\ G_{\perp,r} &= \Sigma_\perp \cdot \mathbf{F}_{\perp,r} \circ (V^\top \bar{V}_\perp + \bar{V}^\top V_\perp) \\ G_{\perp,\perp} &= \bar{\Sigma}_\perp + 2\Sigma_\perp \cdot \mathbf{F}_{\perp,\perp} \circ \text{sym}(V_\perp^\top \bar{V}_\perp) \end{aligned} \quad (56)$$

To identify the dominant bias term, we simplify these blocks with the following observations:

1. Since the loss function only depends on the Top- r components, the upstream gradient $\bar{V}_\perp = 0$ and $\bar{\Sigma}_\perp = 0$, which leads to $G_{\perp,\perp} = 0$ and $V^\top \bar{V}_\perp = 0$.
2. Assume the Top- r singular values are significant while the others are negligible, i.e., $\sigma(\Sigma) \gg \sigma(\Sigma_\perp)$. Therefore, $G_{\perp,r}$ is negligible since scaled by Σ_\perp .

Focusing on $G_{r,\perp}$, we further approximate \mathbf{F} . For indices $i \leq r$ and $j > r$, the approximation $\sigma_i \gg \sigma_j \simeq 0$ yields:

$$(\mathbf{F}_{r,\perp})_{ij} = \frac{1}{\sigma_i^2 - \sigma_j^2} \simeq \frac{1}{\sigma_i^2} \implies \mathbf{F}_{r,\perp} \simeq \Sigma^{-2}. \quad (57)$$

Substituting back into $G_{r,\perp}$:

$$G_{r,\perp} \simeq \Sigma \cdot (\Sigma^{-2}) \circ (\bar{V}^\top V_\perp) = \Sigma^{-1} \bar{V}^\top V_\perp. \quad (58)$$

Based on the derived interaction block, the explicit form of the bias \mathcal{E} is given by the projection of the noise coupling term back to the input space:

$$\mathcal{E} \simeq U G_{r,\perp} V_\perp^\top = U \Sigma^{-1} \bar{V}^\top (I_d - V V^\top). \quad (59)$$

To quantify the potential risk, we estimate the upper bound of its magnitude. Let $\bar{V}_{\text{orth}} = \bar{V}^\top (I_d - V V^\top)$ denote the component of the upstream gradient lying in the noise subspace. The magnitude of the bias is bounded by:

$$\|\mathcal{E}\|_F = \|U \Sigma^{-1} \bar{V}_{\text{orth}}\|_F \leq \|U\|_2 \cdot \|\Sigma^{-1}\|_2 \cdot \|\bar{V}_{\text{orth}}\|_F = \frac{1}{\sigma_r} \|\bar{V}_{\text{orth}}\|_F, \quad (60)$$

where σ_r is the smallest singular value in the signal subspace (the r -th singular value). This upper bound implies that the full gradient is prone to numerical instability as $\sigma_r \rightarrow 0$, where the factor Σ^{-1} arbitrarily amplifies orthogonal noise. Our mechanism serve as a spectral regularizer by enforcing $\|\mathcal{E}\| = 0$, effectively filtering out high-variance components to preserve informative signals.

C. Proof Details

C.1. Proof of Theorem 4.2

Proof. The population risk $R(f)$ can be decomposed into independent optimization problems for each pair (i, j) . Let $\Delta_{ij} = f(x_i) - f(x_j)$ be the logit difference. Minimizing Eq. (17) is equivalent to minimizing each pair:

$$\begin{aligned} \min_{\Delta_{ij}} \mathbb{E}_X [\pi_{ij}^*(X) \log(1 + e^{-\Delta_{ij}}) + (1 - \pi_{ij}^*(X)) \log(1 + e^{\Delta_{ij}})] \\ = p_{ij} \log(1 + e^{-\Delta_{ij}}) + (1 - p_{ij}) \log(1 + e^{\Delta_{ij}}). \end{aligned} \quad (61)$$

This objective is strictly convex with respect to Δ_{ij} . The optimality condition is:

$$\frac{\partial \text{Obj}}{\partial \Delta_{ij}} = -p_{ij} \frac{e^{-\Delta_{ij}}}{1 + e^{-\Delta_{ij}}} + (1 - p_{ij}) \frac{e^{\Delta_{ij}}}{1 + e^{\Delta_{ij}}} = 0. \quad (62)$$

With $\sigma(z) = \frac{1}{1+e^{-z}}$, this simplifies to:

$$-p_{ij}(1 - \sigma(\Delta_{ij})) + (1 - p_{ij})\sigma(\Delta_{ij}) = 0 \implies \sigma(\Delta_{ij}) = p_{ij}. \quad (63)$$

Solving for Δ_{ij} yields $\log(p_{ij}/(1 - p_{ij}))$. \square

C.2. Proof of Corollary 4.3

Proof. Consider any point-wise scorer $f \in \mathcal{F}_{\text{point}}$. By definition, the score $f(x)$ depends solely on item x , implying that the predicted score difference $\Delta_{ij} = f(x_i) - f(x_j)$ is a constant scalar independent of the context X . Consequently, the predicted ordering $\text{sgn}(\Delta_{ij})$ is static.

However, under Assumption 4.1, the ground-truth ordering $\text{sgn}(\eta^*(x_i, X) - \eta^*(x_j, X))$ takes opposite values in contexts $X^{(1)}$ and $X^{(2)}$. Therefore, regardless of the specific value to which f converges, f must misclassify the preference relation on at least one of the contexts.

Since the misclassification event occurs with probability at least $\min(\mathbb{P}(X^{(1)}), \mathbb{P}(X^{(2)})) > 0$, the indicator function in the definition of Bipartite Ranking Risk (Definition 3.2) contributes a non-zero value to the expectation. Thus, $\mathcal{R}(f) > 0$. \square

C.3. Proof of Theorem 4.4

Proof. We first bound the empirical Rademacher complexity $\hat{\mathfrak{R}}_S(\ell \circ \mathcal{F}_{\text{point}})$. Given that the loss function ℓ is 1-Lipschitz, by Talagrand's lemma, we have:

$$\hat{\mathfrak{R}}_S(\ell \circ \mathcal{F}_{\text{point}}) \leq \hat{\mathfrak{R}}_S(\mathcal{F}_{\text{point}}). \quad (64)$$

Let $\{\sigma_{u,i}\}$ be i.i.d. Rademacher variables. Following the definition of $\mathcal{F}_{\text{point}}$, let $z_{u,i} = \phi(u, x_{u,i})$ denote the latent representation. The empirical Rademacher complexity of $\mathcal{F}_{\text{point}}$ is:

$$\begin{aligned} \hat{\mathfrak{R}}_S(\mathcal{F}_{\text{point}}) &= \mathbb{E}_\sigma \left[\sup_{\|w\|_2 \leq W} \frac{1}{mN} \sum_{u=1}^N \sum_{i=1}^m \sigma_{u,i} w^\top z_{u,i} \right] \\ &= \frac{1}{mN} \mathbb{E}_\sigma \left[\sup_{\|w\|_2 \leq W} w^\top \left(\sum_{u,i} \sigma_{u,i} z_{u,i} \right) \right] \\ &= \frac{W}{mN} \mathbb{E}_\sigma \left[\left\| \sum_{u,i} \sigma_{u,i} z_{u,i} \right\|_2 \right], \end{aligned} \quad (65)$$

where the last equality follows from

$$\sup_{\|w\|_2 \leq W} w^\top v = W \|v\|_2. \quad (66)$$

Applying Jensen's inequality, we obtain:

$$\hat{\mathfrak{R}}_S(\mathcal{F}_{\text{point}}) \leq \frac{W}{mN} \sqrt{\mathbb{E}_\sigma \left[\left\| \sum_{u,i} \sigma_{u,i} z_{u,i} \right\|_2^2 \right]} = \frac{W}{mN} \sqrt{\mathbb{E}_\sigma \left[\sum_{u,i} \sum_{v,j} \sigma_{u,i} \sigma_{v,j} z_{u,i}^\top z_{v,j} \right]}.$$

Since $\sigma_{u,i}$ are independent with zero mean, the expectation $\mathbb{E}[\sigma_{u,i}\sigma_{v,j}]$ is 1 if $(u,i) = (v,j)$ and 0 otherwise. Thus:

$$\mathbb{E}_\sigma \left[\left\| \sum_{u,i} \sigma_{u,i} z_{u,i} \right\|_2^2 \right] = \sum_{u=1}^N \sum_{i=1}^m \|z_{u,i}\|_2^2 \leq mNB^2, \quad (67)$$

Substituting back, we have $\hat{\mathfrak{R}}_S(\mathcal{F}_{\text{point}}) \leq \frac{W}{mN} \sqrt{mNB^2} = \frac{WB}{\sqrt{mN}}$. Taking expectation over sample S yields result in (23) and (24). \square

C.4. Proof of Theorem 4.5

Proof. Similar to Theorem 4.4, we have:

$$\hat{\mathfrak{R}}_S(\ell \circ \mathcal{F}_{\text{set}}) \leq \hat{\mathfrak{R}}_S(\mathcal{F}_{\text{set}}). \quad (68)$$

The key difference from the point-wise case is the dependency structure: requests are independent samples while items within each candidate set X_u are dependent. Hence, we use one Rademacher variable per request, i.e., $\{\sigma_u\}_{u=1}^N$. Define the set-wise empirical Rademacher complexity:

$$\begin{aligned} \hat{\mathfrak{R}}_S(\mathcal{F}_{\text{set}}) &= \mathbb{E}_\sigma \left[\sup_{\|w\|_2 \leq W} \frac{1}{mN} \sum_{u=1}^N \sigma_u \sum_{i=1}^m w^\top z_{u,i} \right] \\ &= \frac{1}{mN} \mathbb{E}_\sigma \left[\sup_{\|w\|_2 \leq W} w^\top \left(\sum_{u=1}^N \sigma_u \underbrace{\sum_{i=1}^m z_{u,i}}_{=: \bar{Z}_u} \right) \right] = \frac{W}{mN} \mathbb{E}_\sigma \left[\left\| \sum_{u=1}^N \sigma_u \bar{Z}_u \right\|_2 \right]. \end{aligned}$$

Applying Jensen's inequality and expanding the squared norm:

$$\hat{\mathfrak{R}}_S(\mathcal{F}_{\text{set}}) \leq \frac{W}{mN} \sqrt{\mathbb{E}_\sigma \left[\left\| \sum_{u=1}^N \sigma_u \bar{Z}_u \right\|_2^2 \right]} = \frac{W}{mN} \sqrt{\mathbb{E}_\sigma \left[\sum_{u=1}^N \sum_{v=1}^N \sigma_u \sigma_v \bar{Z}_u^\top \bar{Z}_v \right]}.$$

Since σ_u are independent across users with zero mean, the cross terms vanish for $u \neq v$, and $\mathbb{E}[\sigma_u^2] = 1$. Hence:

$$\mathbb{E}_\sigma \left[\left\| \sum_{u=1}^N \sigma_u \bar{Z}_u \right\|_2^2 \right] = \sum_{u=1}^N \|\bar{Z}_u\|_2^2 = \sum_{u=1}^N \left\| \sum_{i=1}^m z_{u,i} \right\|_2^2. \quad (69)$$

We now bound $\left\| \sum_{i=1}^m z_{u,i} \right\|_2^2$ using the latent correlation assumption. For any fixed user u :

$$\left\| \sum_{i=1}^m z_{u,i} \right\|_2^2 = \sum_{i=1}^m \|z_{u,i}\|_2^2 + \sum_{i \neq j} z_{u,i}^\top z_{u,j} \leq mB^2 + m(m-1)\rho B^2 = mB^2(1 + (m-1)\rho),$$

where we used the bound $\|z_{u,i}\|_2 \leq B$ and the correlation condition (25). Substituting this back into the complexity bound:

$$\hat{\mathfrak{R}}_S(\mathcal{F}_{\text{set}}) \leq \frac{W}{mN} \sqrt{\sum_{u=1}^N mB^2(1 + (m-1)\rho)} = \frac{W}{mN} \sqrt{NmB^2(1 + (m-1)\rho)} = \frac{WB}{\sqrt{mN}} \sqrt{1 + (m-1)\rho}.$$

Taking the expectation over S yields (26). Finally, substituting (26) and the number of independent sampling units $T = N$ (at the user level) into the standard generalization bound (22) yields the result in (27). \square

C.5. Proof of Lemma 4.7

Proof. Let $k = |\mathcal{P}_u|$, $\pi_i = \frac{\exp(s_i)}{\sum_{j=1}^m \exp(s_j)}$ be the softmax probability of item i . The gradient of ℓ_{list} w.r.t. any score s_t is:

$$\frac{\partial \ell_{\text{list}}}{\partial s_t} = \begin{cases} -\frac{1}{k} + \pi_t, & \text{if } t \in \mathcal{P}_u \text{ (positive item),} \\ \pi_t, & \text{if } t \notin \mathcal{P}_u \text{ (negative item).} \end{cases} \quad (70)$$

Compute the squared ℓ_2 -norm of the gradient vector $\nabla_s \ell$:

$$\begin{aligned} \|\nabla_s \ell\|_2^2 &= \sum_{t \in \mathcal{P}_u} \left(-\frac{1}{k} + \pi_t\right)^2 + \sum_{t \notin \mathcal{P}_u} (\pi_t)^2 = \sum_{t \in \mathcal{P}_u} \left(\frac{1}{k^2} - \frac{2}{k}\pi_t + \pi_t^2\right) + \sum_{t \notin \mathcal{P}_u} \pi_t^2 \\ &= \sum_{t \in \mathcal{P}_u} \frac{1}{k^2} - \frac{2}{k} \sum_{t \in \mathcal{P}_u} \pi_t + \sum_{t=1}^m \pi_t^2 = k \cdot \frac{1}{k^2} - \frac{2}{k} \pi_{\text{pos}} + \|\pi\|_2^2 = \frac{1}{k} - \frac{2}{k} \pi_{\text{pos}} + \|\pi\|_2^2, \end{aligned} \quad (71)$$

where $\pi_{\text{pos}} = \sum_{t \in \mathcal{P}_u} \pi_t \in [0, 1]$ is the total probability mass on positive items. Since $\|\pi\|_2^2 \leq \sum \pi_i = 1$ and $\pi_{\text{pos}} \geq 0$, the maximum value is bounded by:

$$\|\nabla_s \ell\|_2^2 \leq \frac{1}{k} + 1 \leq 2 \quad (\text{since } k \geq 1). \quad (72)$$

Thus, $\|\nabla_s \ell\|_2 \leq \sqrt{2}$, confirming the loss is $\sqrt{2}$ -Lipschitz regardless of the number of positive items. \square

C.6. Proof of Theorem 4.9

Proof. Pointwise: Let the pointwise model be defined as $z_k = \phi_\theta(u, x_k)$, where ϕ_θ is a continuous mapping. For deep neural networks with bounded weights, ϕ_θ is Lipschitz continuous. There exists a constant K such that:

$$\|z_i - z_j\| = \|\phi_\theta(x_i) - \phi_\theta(x_j)\| \leq K\|x_i - x_j\| \quad (73)$$

Substituting the input decomposition, we have $\|x_i - x_j\| = \|d_i - d_j\|$. Since the discriminative variations are minute, the Euclidean distance between outputs is constrained to be small. Assuming $\|z_i\| = \|z_j\| = 1$, the squared distance is related to correlation by $\|z_i - z_j\|^2 = 2(1 - \rho_{\text{point}})$. The Lipschitz condition implies:

$$2(1 - \rho_{\text{point}}) \leq K^2\|d_i - d_j\|^2 = \epsilon \quad (74)$$

Thus, $\rho_{\text{point}} \geq 1 - \frac{\epsilon}{2} \rightarrow 1$. The pointwise network preserves the topological collinearity of the input space, leading to an update conflict where gradients cannot effectively separate z_i and z_j .

Setwise. Let the setwise model be defined as $z_k = \phi_\theta(u, x_i, X_u)$, where X_u is the candidate set. The set-wise attention mechanism computes the representation as:

$$z_k = W_V \left(x_k - \sum_{i \in X_u} \alpha_{k,i} x_i \right) \quad (75)$$

To maximize the margin $s_i - s_j$, the gradient descent encourages the attention mechanism to ignore common features and extract differences. Specifically, the aggregated context vector approximates the common component \mathbf{c} . The effective transformation becomes a projection onto the subspace orthogonal to \mathbf{c} :

$$z_i \rightarrow \mathcal{P}_{\mathbf{c}^\perp}(x_i) = \mathbf{d}_i, \quad z_j \rightarrow \mathcal{P}_{\mathbf{c}^\perp}(x_j) = \mathbf{d}_j \quad (76)$$

By removing the dominant common component, the output representations are dominated by the discriminative terms \mathbf{d}_i and \mathbf{d}_j . Assuming the distinct features are i.i.d., they are orthogonal in high-dimensional space ($\mathbf{d}_i \perp \mathbf{d}_j$). The resulting correlation is:

$$\rho_{\text{set}} \propto \mathbf{d}_i^\top \mathbf{d}_j \rightarrow 0 \quad (77)$$

Hence we conclude that $\rho_{\text{set}} \ll \rho_{\text{point}}$. The setwise architecture breaks the correlation bottleneck by dynamically filtering out the shared context, thereby effectively minimizing the listwise ranking loss. \square

D. Construction of Datasets

RecFlow. RecFlow (Liu et al., 2025) logs user behavior throughout a multi-stage industrial recommendation pipeline, making the candidate sets at intermediate stages directly observable rather than inferred from final exposure alone. We follow the dataset protocol and use the 2nd period from Feb 5th to Feb 18th, which contains 3,308,233 requests. Our experiments intercept the pipeline at the re-ranking stage. For each request, we take the top 120 items passed from the upstream ranking module and retain their original order as a positional reference feature. The model consumes item-side attributes, including video ID, category, and author-related fields such as upload type, age, gender, and device type, together with a user-context sequence of fixed length 50 that captures recent interactions.

MIND. MIND (Wu et al., 2020) is a large-scale benchmark derived from Microsoft News impression logs. Each labeled sample follows the format $[uID, t, ClickHist, ImpLog]$, where *ImpLog* enumerates the news articles displayed in an impression with click labels and *ClickHist* records the user’s previously clicked news IDs in chronological order. Each news article provides a news ID, title, abstract, body, and an editor-assigned category; the release also includes extracted entities linked to WikiData, along with knowledge triples and embeddings. We treat each impression as a request and use the displayed articles in *ImpLog* as the base candidate set. Beyond the real exposures, we augment the candidate set with additional negatives drawn from the full news pool: some are sampled uniformly at random, others are selected from globally popular articles, and the remainder are chosen from similar item set.